Compact And Scalable Large Vortex Array Generation Using Azocarbazole Polymer And Digital Hologram Printing Technique

Jackin Boaz Jessie (jackin@kit.ac.jp)
Kyoto Institute of Technology
Shirai Masaki
Kyoto Institute of Technology
Haginaka Honoka
Kyoto Institute of Technology
Kenji Kinashi
Kyoto Institute of Technology
Naoto Tsutsumi
Kyoto Institute of Technology
Wataru Sakai
Kyoto Institute of Technology

Research Article

Keywords: optical vortex, computer generated holography, hologram printing, photoinduced birefringence, integrated device

Posted Date: December 6th, 2021

DOI: https://doi.org/10.21203/rs.3.rs-1136355/v1

RESEARCH

Compact and scalable large vortex array generation using Azocarbazole polymer and digital hologram printing technique

Jackin Boaz Jessie[1*], Shirai Masaki[2], Haginaka Honoka[3], Kenji Kinashi[4*], Naoto Tsutsumi[4] and Wataru Sakai[4]

[*]Correspondence: jackin@kit.ac.jp; kinashi@kit.ac.jp
[1]Materials Innovation Laboratory, Kyoto Institute of Technology, Kyoto, Japan
[4]Faculty of Materials Science and Engineering, Kyoto Institute of Technology, Kyoto, Japan
Full list of author information is available at the end of the article

Abstract

An integrated device capable of generating large number of multiplexed optical vortex beams with arbitrary topological charges is considered as one of the crucial requirement for driving information photonics forward. Here we report a simple method for simultaneous generation of 100 multiplexed optical vortex beams from a polymer film of size $1mm^2$ and thickness of $30\mu m$. This is achieved through a combination of computer generated holography, digital hologram printing and photoisomeric polymers. When the fabricated sample is illuminated with a collimated laser beam, a pre-determined vortex array with arbitrary topological charge is emitted. The polymer film easy to synthesise and exhibits good diffraction efficiency and long retention time.

Keywords: optical vortex; computer generated holography; hologram printing; photoinduced birefringence; integrated device

Introduction

Though photonics offers higher speed, large parallelization, low noise and low energy consumption compared to their electronic counterparts, they have enjoyed limited success in information processing applications. The main reason is the bulky system resulting from the assembly of free-space optical components (lenses, mirrors, beam-splitters, light modulators, etc) on an optical bench. This leads to the cost and the size footprint of the system increasing non-linearly with system performance ie., the system lacks scalability. Optical vortex beam generators, (especially vortex array generators), are no exception to the above snag. Hence photonics technology demands a transition from the existing table-top format systems to an on-board or on-chip format system that is capable of driving the system footprint to scale linearly with the performance output. This requires novel materials and methods for denser integration of optical functions and has resulted in the emergence of a new field on its own known as 'Integrated optics'. Optical vortex generators have also undergone significant improvements in optical integration in the past decade. In this paper we report a simple and novel technique for generation of large vortex array generation from a hologram of size $1mm^2$.

Integrated vortex array generators

The class of optical vortex generators that emit multiple optical vortex beams simultaneously from a single input beam has attracted huge interest in the information

processing community. These multiple vortice emissions take any one of the following form, i) each emitted vortex beam takes a unique pre-defined position in space and are spatially separated from each other known as a vortex array or vortex lattice, and ii) all vortex beams exist co-axially and are decoupled at the detection stage using a mode-sorting or mode-demultiplexing arrangement. 'Vortex arrays' are more beneficial for information processing operations since each vortex beam in the array can independently interact in space with a medium/other-vortex and be modulated individually to realize a required function. On the other hand, co-axially emitted modes are useful for information transmission as they can be coupled into fiber or launched into free-space. Computer generated holography (CGH) using spatial light modulators (SLM) are the most popular technique used for simultaneous generation of large number of multiplexed vortex beams [1,2]. These systems are assembled on an optical bench making it significantly bulky and non-scalable. Several techniques for minaturisation and optical integration were developed and reported in the past decade. The following is a short review on existing integrated devices and methods for optical vortex array generation.

Silicon-on-insulator (SOI)

Considering multiplexed vortex generators, most of the research on silicon photonics are focussed on emission of coaxially superposed vortex beams [3, 4], which are suitable for communication purposes. There are only a few existing reports that demonstrate vortex array generation. Cai et al [5] have reported multiple vortex beam generation by fabricating silicon micro ring resonators which support whisphering gallery modes (WGM) carrying orbital angular momentum (OAM). The input light is coupled into the micro rings through a waveguide and the generated vortex beams were coupled out to freespace by inscribing angular grating structures on the inner wall of the ring structures. The device is OAM tunable by changing the injected wavelength and operates in the range of 1470nm to 1580nm. A 1D array of 3 vortex beams were generated by fabricating three identical ring structures on the same substrate. Vortex lattice generation using the principle of 'three plane wave intereference', implemented by fabricating three parallel waveguides with etched tilt gratings on a SOI plafrom has been reported by Du et al [6]. Though silicon photonics has the advantage of advanced tooling (from the electronic industry), large vortex array generation (100 or larger OAM modes) has not been reported yet. Moreover, silicon photonics works only in telecomwavelength ($1.5\mu m$ to 2.5 μm) whereas a lot of interesting optical OAM events/phenomena occur in the visible wavelength ($400nm$ to $700nm$) regime.

Metasurface

Metasurfaces, also known as 2D metamaterials are a distribution of sub-wavelength structures, either inscribed or deposited on a 2D substrate. A plasmonic metasurface fabricated using an array of gold nano antennas and capable of simultaneously emitting four vortex beams with different topological charges ranging from l=1 to l=4 was reported by Yue et al [7]. Maguid et al. have combined the properties of harmonic response and geometric phase of metamaterials to fabricate a harmonic response geometric phase metasurface [8]. Six vortex beam modes with topological

charges l=1,2,3,-1,-2,-3 (harmonics) are generated when the metasufrace is illuminated with a polarized Gaussian beam. Metasurface fabricated by milling nano holes in gold substrate capable of modulating both the amplitude and phase of the input beam was reported by [9]. A 6 × 6 array of vortex beam with topological charge ranging from l=-4 to l=3 was demonstrated. Ren et al. have introduced the concept of OAM conserving meta-hologram where the output is a OAM-pixelated image [10]. The metasurface when illuminated with a OAM beam, reconstructs a OAM-pixelated image where each pixel possesses a topological charge in accordance with the charge of input beam. Multiplexing multiple vortex arrays was recently reported by Jin et al [11]. Three vortex arrays were angularly multiplexed using the principle of superposition of holograms and implemented using a geometric metasurface. Three distinct vortex arrays (l=-2 to l=3) are generated from the same metasurface when illuminated from three different angles. The vortex arrays discussed so far had a 2D profile (each vortex beam in the array is arbitrily positioned in the lateral (x-y) plane), but Huang et al. reported the possibility of generating a 3D vortex array (where the profile of each vortex beam can be made to arbitrarily vary in the longitudinal (z) axis) [12]. A dielectric metasurface was fabricated to generate a 5×5 3D vortex array ($l = -8tol = 0$) which exhibits different beam profile in the z-direction. Another 3D vortex array generation method that is sensitive to the input wavelength was reported by Jin et al [13]. Two different 3×3 3D vortex arrays were generated from the same metasurface only by switching wavelengths Reflection type metasurfaces, known as 'meta-reflectarray' used for vortex array generation was reported by Liu et al. [14]. A 5x5 vortex array with topological charge varying from $l = -4$ to $l = +12$ was generated The reflection configuration helps to achieve a maximum diffraction efficiency of 70% and a broad bandwidth ranging from 1250nm to 1750nm. To the best of our knowledge, generation of a large vortex array (∼100) with higher topological charges has not been reported yet. The reason can be attributed to the challenges in fabricating sub-wavelength structures that could execute larger phase modulation, higher harmonic generation or extended spin-orbit angular momentum exchange.

Computer generated holography

Here we discuss the existing techniques for vortex array generation that are based on computer generated holograms that are scalable with small size footprint and are eligible for optical integration. Zhuang et al [15] have reported the generation of vortex array of size 3 × 3 with topological charge ranging from l=-2 to l=3 using a micro CGH fabricated on lithium niobate crystal using direct laser writing. Emission of vortex array from holographically recorded vortex lattices on nematic liquid crystal cells [16] and polymer dispersed liquic crystal films [17] has been reported. Here the recorded sample is illuminated with an array of circularly polarized beams inorder to generate a corresponding array of vortex beams. It is also worth discussing a few single vortex generators based on CGH, as they are very close to the proposed work. Carpentier et al, [18] have reported generation of optical vortex of charge l=1 to l=4 using a CGH of size $5mm^2$ recorded on a photographic film using optical reduction. Computer generated holograms recorded inside glass substrate by femtosecond laser pulses for generation of optical vortices was reported by Guo

et al, [19]. Large vortex array generation employing scalable and compact CGH's has not been reported yet. In this paper we report a very simple yet efficient CGH based method that can emit a 10×10 vortex array from polymer sample size of $1mm^2$

Material and Methods

The purpose here is to record computer generated hologram on a small area of a polymer film, which (later) when illuminated with a Gaussian beam emits an array of vortex beams with arbitrary topological charges. The above mentioned is executed as a four step process consisting of a) sample synthesis, b) hologram computation, c) hologram printing and d) hologram reconstruction, as shown in Figure.1. The material chosen for hologram recording is Azocarbazole polymer which is fabricated as a thin film. The computed hologram pattern is a superposition of multiple fork gratings each of which correspond to a single vortex beam. The computed pattern is then optically transferred to the polymer film as refractive index modulation. The sample when illuminated with a Gaussian beam emits an array of vortices in accordance with the recorded pattern. Each step in the process is explained below,

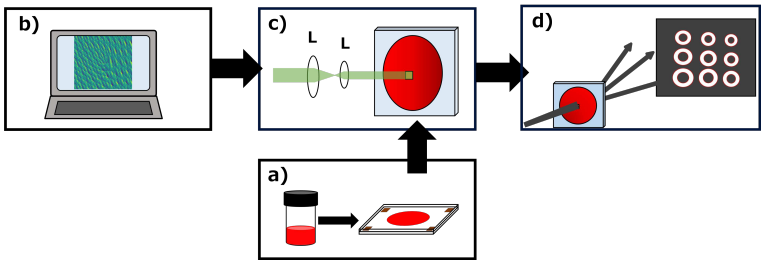

Figure 1 Schematic showing the steps involved in devising the vortex array generator, a)Synthesis of hologram material (Azocarbazole polymer), b)Digital computation of hologram pattern capable of reconstructing the vortex array, c)optical transfer of the computed pattern onto the synthesised material (digital hologram recording) and d) reconstruction of vortex array by illuminating the recorded digital hologram using a Gaussian beam

Photoisomerization

The sample being prepared to be used for hologram recording works on the principle of photo induced birefringence. This sample material when exposed to light radiation exhibits photoisomerization by switching between a trans and cis state known as trans-cis isomerization. When illuminated with a light pattern with alternate bright and dark regions (fringe pattern), only the molecules in the sample that are exposed to light radiaion (bright region) undergo isomerization as shown in Fig.2(a,b). Once the light is turned off, these exposed molecules get oriented in a direction perpendicular to the polarization of the input light beam as shown in Fig.2(c). These orientations remain intact until perturbed again by heat or a strong radiation and hence the recorded change is permanent. The recorded molecular orientation induces anisotropy and hence the material becomes birefringent in the exposed region. So a light polarized in a suitable direction experiences a difference in refractive index when passing through the exposed (oriented) and un-exposed

areas. Thus by spatially modulating the incident light intensity distribution in accordance with the pattern to be transfered, and by exposing the sample onto the radiation, the corresponding pattern is recorded on the material as refractive index modulation (Δn) as shown in Fig.2(c).

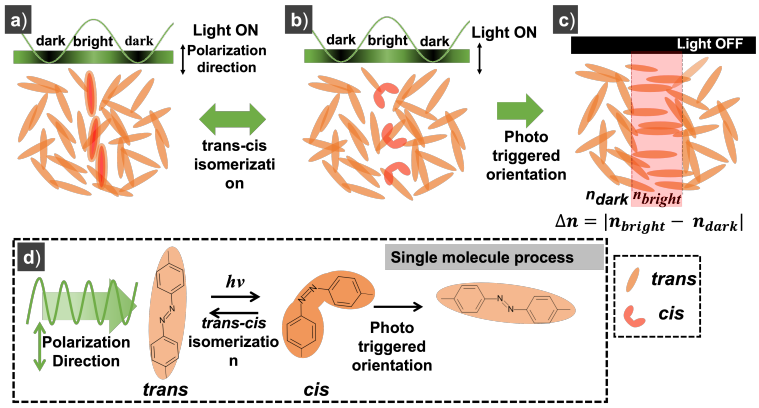

Figure 2 Schematic showing the process involved in the transfer of light intensity pattern as refractive index modulations (Δn) on the material sample utilizing the phenomena of photoinduced isomerization. a,b) cis-trans isomerization cycle, c) photo-triggered orientation. d) schematic of the photoinduced isomerization process at a single molecule level.

Sample synthesis

The material that serves as the photoisomeric medium in this experiment is an azoderivative called as azocarbazole. It is made of an azobenzene-functionalized copolymer, poly(CACzE-MMA), which is composed of 3-[(4-cyanophenyl)azo]-9H-carbazole-9-ethanol (CACzE), methyl methacrylate (MMA), CACzE, and diphenyl phthalate (DPP), as shown in Fig.3(a). The procedure for synthesis of poly(CACzE-MMA) and CACzE was reported earlier by Kinashi et al [20]. DPP was purchased from a commercial source (Tokyo Kasei Co.), and used as a plasticizer to decrease the glass transition temperature T_g of the azocarbazole composite. In this study, the composition of polymer/CACzE/DPP was fixed at 45/15/5 by weight. The mixture was first stirred in tetrahydrofuran (THF) for 48 hours, and then cast on a hot plate at 70^{o}C for another 48 hours. The resulting polymeric powder was pressed between two glass substrates at 180^{o}C as shown in Fig.3(b). Polyimide (or Teflon) spacers were used to adjust the thickness of the working layer to be 35μm. The size of the sample was 3cm $\times$ 3cm and a photograph of the synthesized sample is shown in Fig.3(c). The procedure mentioned by Kinashi et al [20] was used to experimentally measure the haze value of the sample. Haze value is a measure of the the transpareny of the sample and was found to be 1.2 at 633 nm wavelength, which indicates high transparency. The stability of the recorded grating pattern (retention time) for the synthesized sample was experimentally obtained using the procedure reported earlier [20]. The measured retention was rate 70% after after a period of 50 days, which indicates good stability at room temperatures.

Hologram computation

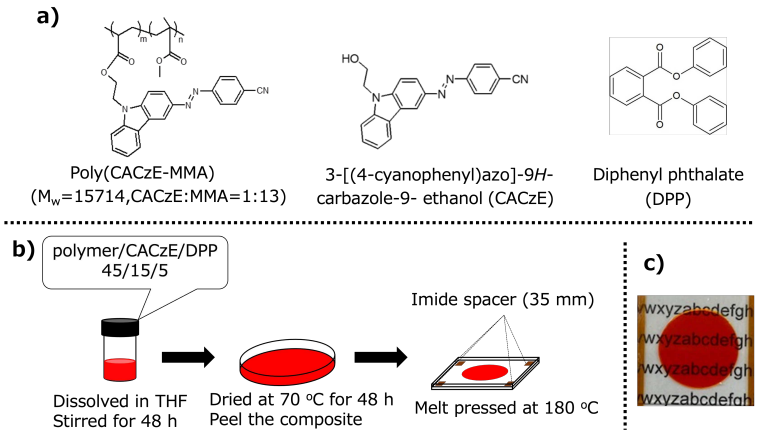

Figure 3 a) Chemical structure of the materials used for sample preparation, b) (left to right) the three steps involved in the polymer film fabrication and c) photograph of the fabricated sample placed on top of printed alphabets, showing good transmittance.

Since the amplitude and phase of a vortex beam can be well defined as a mathematical function, numerical simulation or diffraction calculation (as in the case of conventional holography) is not required. Instead, it is simply required to construct 2D matrices that represent the phase of the vortex beam crosssection (spiral phase) and a carrier beam corsssection (linear phase). Adding these two matrices and wrapping them by 2π gives rise to the hologram pattern H_1 (also known as fork grating) as shown in Fig.4(a,b). The phase gradient of the carrier beam defines the position where the vortex beam will be reconstructed. (Vortex beams are observed as a donut shaped intensity distribution and hence are represented as circular rings in Fig.4). The steeper the phase gradient of carrier beam larger will be the diffraction angle during reconstruction. This results in the vortex beam being reconstructed farther from the 0^{th} order beam. This is graphically presented in figure 4, where sub-figure (b) represents a carrier with larger phase gradient than the one in sub-figure (a). Hence the reconstructed vortex shown in sub-figure(b) is located at a farther position from the 0^{th} order, compared to the vortex in sub-figure(a). Thus by choosing an appropriate carrier beam to be added with each vortex beam, an array of non overlapping vortex beams can be created. In other words, each vortex beam emerges from the hologram at a slightly different angle during reconstruction and is also known as 'angular multiplexing'. Multiple holograms $(H_1, H_2, ...H_n)$ can be computed by adding each vortex beam with a different carrier beam. Adding all these multiple holograms together $(H_1 + H_2 + ... + H_n)$ gives rise to a single multiplexed hologram as shown in Fig.4(c). The multiplexed hologram is capable of reconstructing each of the recorded vortices in its appropriate position as a 2D array (Fig.4-c)

Digital Hologram printing

The optical setup used to transfer the computed hologram onto the fabricated polymer film is shown in Fig.5. The beam from a laser source of wavelength 532nm is filtered and collimated and send into an SLM. The SLM displays the computed

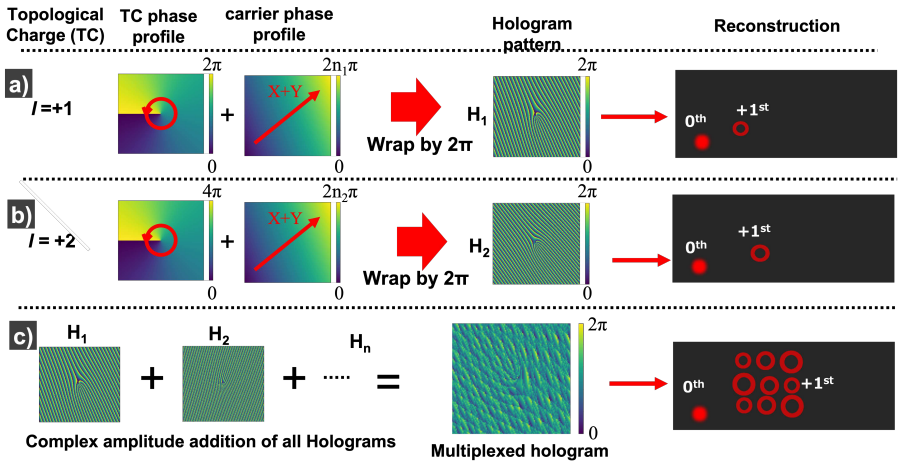

Figure 4 a) (left to right) The spiral phase profile corresponding to TC $l = +1$ is added to a linear phase profile (carrier) and then wrapped by 2π to generate the hologram pattern H_1, which then reconstructs the vortex beam of TC $l = +1$, b) The spiral phase corresponding to TC $l = +2$ is added to a linear phase profile (carrier) and then wrapped by 2π to compute the hologram pattern H_2, which then reconstructs the vortex beam of TC $l = +2$, c) The phases of holograms $H_1, H_2, ..., H_n$ are added together to generate the multiplexed hologram, which when reconstructed emits all the corresponding vortices as an array.

hologram pattern and the beam reflected back from the SLM is modulated accordingly in amplitude. The SLM used is Holoeye LC-R 1080 which is configured to work in amplitude only mode using a combination of quarter wave plate and polarizing beam splitter (PBS) as shown in Fig.5. The sample is mounted on a three axis translation stage at a distance parallel to and facing the SLM. The light reflected from the SLM reaches sample through a set of demagnifying and imaging lenses. Though only two lenses (L_3&L_4) are shown in Fig.5 for simplicity, and it should be noted that is actually composed of 7 lens elements to cancel out aberrations. It is this imaging optics that enables the efficient transfer of the pattern displayed by the SLM onto the sample with a 10x demagnification. Raytracing simulations (zemax software) showed the spot size on the imaging plane to be $0.8\mu m$ with a tolerance of $20\mu m$ in focal shift. So it is necessary to place the sample at the focal plane of the lens with an accuracy of $20\mu m$. This is realized by mounting the sample on a high accuracy motorized 3-axis motion stage equipped with a encoder based feedback. The power of the laser beam at the recording plane was $32mW/mm^2$ and the exposure time for recording is 5 seconds (single exposure). The recorded refractive index modulations on the sample were then verified using a phase contrast microscope.

The computed fork grating of topological charge $l = -10$ and the corresponding phase contrast microscopic images of sample after recording are shown in Fig.6. Phase contrast microscopic images showing the effect of shift in sample position (from the best focus) on the accuracy of the printed hologram, is shown in Fig.7. Hence it is necessary to ensure accuracte positioning of the sample with respect to the imaging optics, which is achieved by mounting the sample on a motion stage. The size of each pixel on the SLM is $8\mu m$ which is demagnified 10-times onto the polymer sample resulting in a pixel pitch of $0.8\mu m$. The displayed hologram consisted of 1200 x 1200 pixels which results in a printed hologram of size 0.960 mm

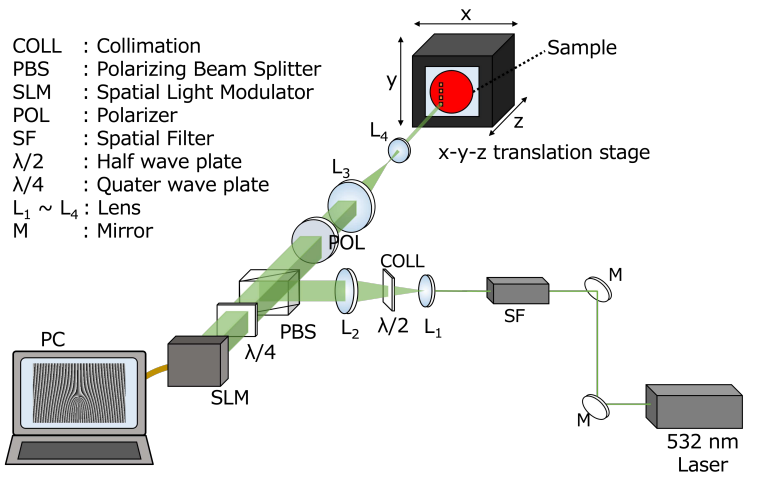

Figure 5 Schematic of the optical printing setup built on the optical table for digital hologram printing.

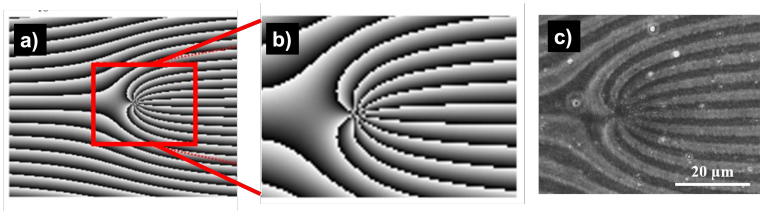

Figure 6 a) The digitally computed hologram pattern corresponding to topological charge $l = -10$ b) magnified image of the region of interest from the center c) phase contrast microscopic image from the recorded sample corresponding to the region of interest

$\times$ 0.960 mm in size. The printed pixel pitch and size were verified experimentally to be in agreement with the numbers mentioned above, through microscopic measurements.

Results

The reconstruction experiments were carried out using the optical system shown in Fig.8. It is a simple system designed with the purpose of generating a collimated beam of diamter $1mm$ that matches with the size of the hologram printed. Since the fabricated sample is highly transmissive in the red region, a laser source of wavelength 640 nm was used. Vortex beams are emitted in all diffraction orders $(-\infty ... \infty)$ when illuminated since the hologram (grating) here functions a thin grating that belongs to the Raman-Nath regime. It should be noted that even though the sample film had a thickness of $35\mu m$, it does not qualify as a volume Bragg grating since the recording is done using a single beam in a imaging configuration. It is only the first order diffracted that is of importance since it possesses most of the power and all of the information. The zeroth-order (I_0) and first-order (I_{-1}, I_{+1}) diffracted beam intensity is measured using photodiodes and the diffraction efficiency η is calculated using the folmula shown in Eq.1. Figure.9 is a plot of the diffraction efficiency with

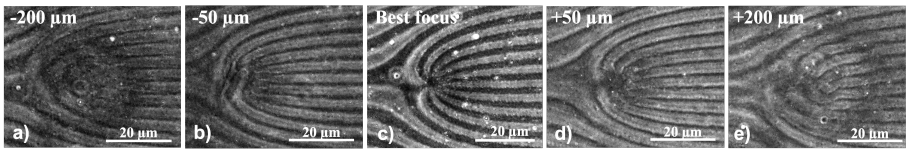

Figure 7 Phase contrast microscopic images (contrast enchanced) showing the printed accuracy being affected by sample position with respect to best focus. a,d) 200μm away from best focus, b,d) 50μm away from best focus and c) at best focus

respect to TC of emitted vortex beams. It can be concluded that the diffraction efficiency achieved is close to the maximum theoretical limit of Raman-nath regime and does not change with topological charge.

$$\eta = \frac{I_{+1}}{I_{+1} + I_0 + I_{-1}} \tag{1}$$

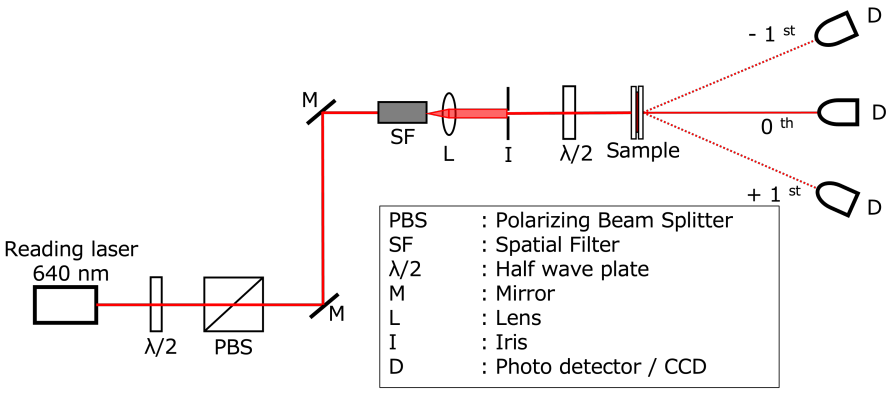

Figure 8 Schematic of the optical setup used for reconstructing the printed holograms and for capturing the reconstructed light intensity pattern

Figure.10 shows the 0^{th} and 1^{st} order diffracted beams captured using a charge-coupled device (CCD) sensor, from holographic reconstructions using the optical setup shown in Fig.8. The recorded pattern in these holograms correspond to a single vortex beam each with a different topological charge ($l = -4, -10, -20, -50, -100, -125$). The increase in radius of the reconstructed donut pattern with increasing topological charge can be observed from Fig.10. It can also be concluded that the largest topological charge that can be reconstructed with high fidelity from the hologram of size $1mm^2$ is l=-50. In order to verify the topological charge of the reconstructed optical vortices an Mach-Zehnder type interferometer was constructed as shown in Fig.11. The interference pattern corresponding to the superposition of the generated vortex beam and a Gaussian beam (with a small divergence) was captured on the CCD sensor. The captured pattern that correspond to vortex beam with topological charges $l = -5, -10, -25$ are shown in Fig.11(b,c,d)

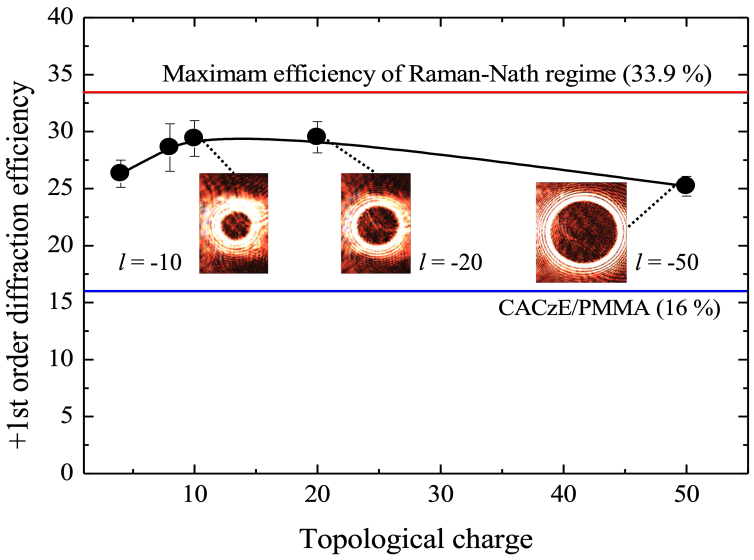

Figure 9 The plot of diffraction efficiency with different topological charge of the vortex beam. Diffraction efficiency close to the theoretical maximum for Raman-Nath regime (red line) has been achieved

respectively. The number of the fins in the interferograms matches with the topological charge of the vortex hologram used, which confirms the correctness of vortex beams generated.

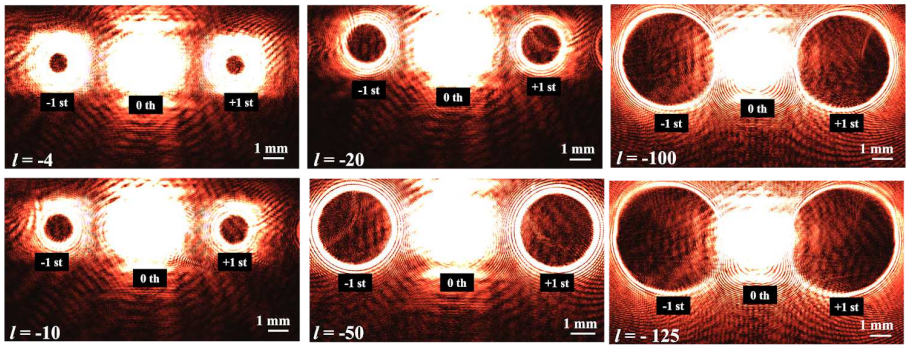

Figure 10 Reconstructions from single vortex beam generating holograms captured using a CCD sensor. The images show the $0^{th}, +1^{st}, -1^{st}$ reconstructed diffraction orders for different topological charges (see embedded label for details)

Multiplexed hologram patterns corresponding to a 6×6 and 10×10 vortex array were recorded on the polymer and then subjected to reconstruction tests. Both the fabricated holograms had the same size $1mm^2$ and the same number of pixels 1200×1200 mentioned earlier. The reconstructions were captured directly using a CCD camera at a distance of 5cm from the sample and are shown in Fig.12(a,c). The horizontal and vertical lines seen in the images are due to a tiled capture procedure adapted to circumvent the issue of vortex array size being larger than the CCD sensor area. Figures.12(b,d) represent the reconstructions captured from a black screen placed at a distance of 10cm from the hologram sample using a photographic

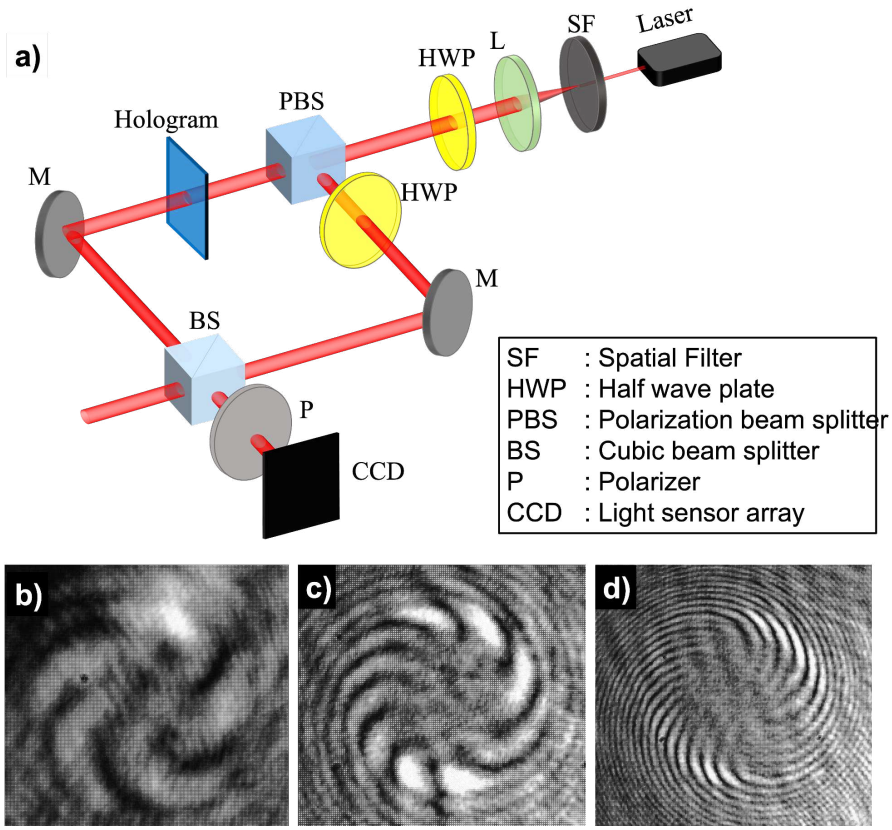

Figure 11 a) Schematic of the optical setup used to capture the interference pattern between Gaussian beam (with a small divergence) and vortex beam generated by a hologram. Interference pattern captured at the CCD plane that corresponds to a vortex hologram of topological charge b) $l = -5$, c)$l = -10$ and d)$l = -25$. The number of fins in the interference pattern matches with the topological charge

camera. These images show the 0^{th}-order and $+1^{st}$-order reconstructed beams. A few donut shaped pattern seen close to the 0^{th} order beam correspond to the weak autocorrelation term in holographic reconstruction. From the above experimental results it can be concluded that a 10×10 vortex array with arbitrary topological charge upto $l = -10$ can be successfully generated from a sample of size $1mm^2$

Discussion

Maximum array size and topological charge

Hologram recording and reconstruction experiments were performed for larger array sizes than the one reported above (10×10) upto 12×12. This resulted in an overlap of $+1^{st}$ and $+2^{nd}$ order reconstructed vortex arrays. So, it is required to use a carrier phase with a much steeper gradient inorder to further separate out the $+1^{st}$ and $+2^{nd}$ diffraction orders, inorder to avoid the overlap. This demands a smaller pixel pitch but the current hologram printing system is limited to a pixel pitch of $0.8\mu m$. The total number of vortex beam in the array also depends on the topological charge of each vortex. Since larger topological charges diverge fast and consumes larger space, it is required to reduce the number of vortices in the array inorder

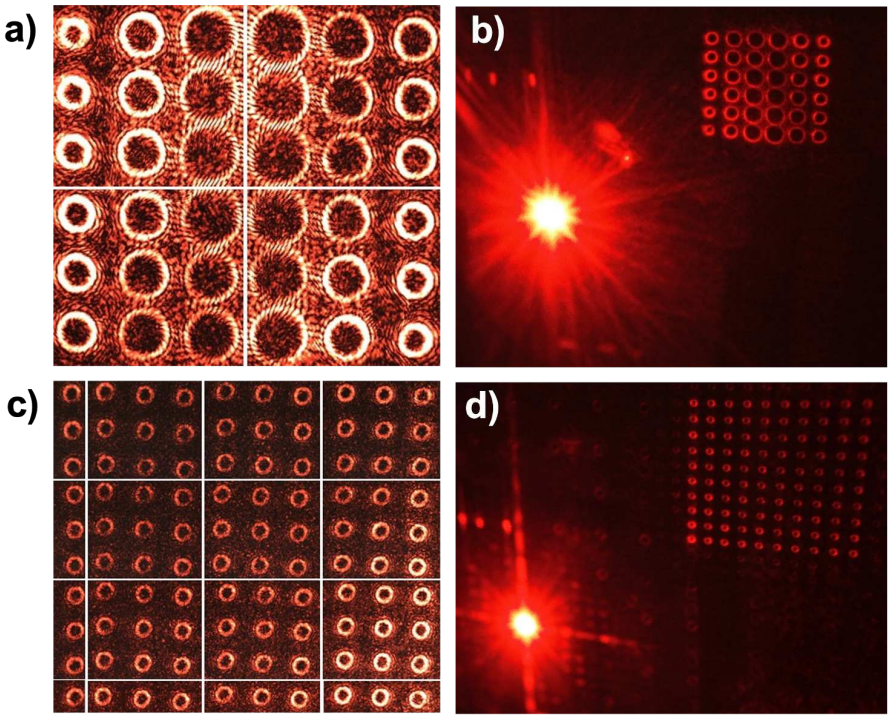

Figure 12 Reconstructions captured from $+1^{st}$ order diffracted beams of multiplexed holograms. A 6×6 vortex array consisting of topological charges $l = -6, -12, -24$ a) captured directly on a CCD sensor, b) captured from a screen using a camera showing the 0^{th} order and $+1^{st}$ diffracted beams. A 10×10 vortex array consisting of topological charges $l = -10$ c) captured directly on a CCD sensor, d) captured from a screen using a camera, showing the 0^{th} order and $+1^{st}$ diffracted beams.(The white horizontal and vertical lines in the CCD images (a,c) are due to a tiled capture procedure adapted due to the CCD sensor area being smaller than the recostructed vortex array size)

to avoid overlap. The same applies to the largest topological charge that can be successfully generated. Beams with a large topological charge consume larger area and also exploits a steeper spiral phase gradient which inturn demands a smaller pixel pitch. Hence the topological charge is limited to $l = -50$ for a high fidelity reconstruction in the reported system. The current limitations can be overcome to a certain extent by adapting a latest available SLM which boasts a pixel pitch of $3.75\mu m$.

Further possibile improvements

The currently reported diffraction efficiency can be further increased by adapting a volume hologram (thick hologram) recording configuration [21] . These are also called as Bragg holograms and requires the presence of another beam (as reference) during recording. Such a two beam recording can be performed using the currently reported optical system with minimal modification. Diffraction efficienciency of 68% has been reported for the same azocarbazole sample for such a two beam hologram recording at a wavelength of 532 nm [22]. Since only the +1 diffraction order is present while reconstructing a volume hologram, there will be no overlap (with $+2^{nd}$ and higher orders) which helps in increasing the number of vortices in array. It is also possible to further increase the number of pixels of the hologram further

(from the currently reported 1200×1200), which could inturn increase the purity of vortex modes reconstructed. For this a hologram stitching procedure is to be implemented by placing the sample on a x-y motion stage. Recording such larger stitched hologram to understand its effects on mode purity is one of the future goals in this research. It is also important to note that the azo polymer used in this research exhibits photoinduced anisotropy through photoisomerization and molecular reorientation. The material anisotropy can induce geometric phase in the propagating beam and thereby opening up the possibility of vector beam mode generation. But a precise understanding and control of material anisotropy during recording is required.

Dynamic generation of vortex array

An important drawback of the proposed method is its inability to generate vortex arrays dynamically in realtime as is done using an SLM. Though the reported azo polymer can be optically erased and rewritten, the rewritable speed is quite slow ($\tilde{5}$ sec) for realtime operation [20]. Generally, information processing applications demand realtime updateable generation of beam modes which makes SLM as the most popular choice. But another strategy for dynamically generating modes is to do a static generation followed by a dynamic modulation. In other words, the generation process and dynamic modulation process should be separated out but be allowed to function together inorder to realize dynamic generation. For example, optical functions such as multicasting, switching, coupling, mode mixing etc can be employed to generate any arbitrary vortex array pattern, from a basic set of fixed static vortex array generated. Integrated optics has shown significant progress in the above mentioned direction and will be the key player in realizing such a strategy.

Future prospects of vortex beams for information processing

As Moore's law is closing-in on its saturation limit, several abstract computing paradigms (machine learning, artificial intelligence, etc) are starting to feel the stress. These computing paradigms are currently implemented on the transistor based Von Neumann computing framework and an alternate framework is actively sought after. Photonics is considered as one of the promising candiate to succeed as an alternate framework. Today, photonics technology dominates electronics in the long distance information transmission regime, but it struggles to catch up with electronics in the information processing regime. The main reason is the difficulty to 'localize' or confine photons (at the nanoscale) to a predetermined position in space and time, as we do with electrons (charge). So, photonics based methods are generally used as an non-conventional information processing (computing) platform for tasks such as optical image processing, optical neural networks, information display etc, that do not demand localizing photons. Considering light, it is usually the amplitude, phase, wavelength and polarization degrees of freedom of light beams that are used as information carriers/modulators. Recent developments have revealed that the orbital angular momentum states (OAM) of light (known as vortex modes) is another degree of freedom and possesses better information processing potentials. The capabilities are attributed to its robust propagation characteristics and the unbound limit of orthogonal OAM states which helps in lossless transmission

and the parallel processing of huge volumes digital data. The above mentioned potentials along with the availability of state-of-art fabricataion techniques for vortex beam geneartors, has rekindled interest in the non-conventional optical computing frameworks mentioned earlier. We believe this research work will be a small stepping stone in this direction.

Acknowledgements
Not applicable

Funding
Not applicable

Abbreviations

CGH	-	Computer generated holography
WGM	-	Wishpering gallery modes
OAM	-	Orbital angular momentum
SOI	-	Silicon on insulator
SLM	-	Spatial light modulator
MMA	-	Methyl methacrylate
DPP	-	Diphenylphthalate
THF	-	Tetrahydrofuran
CCD	-	Charge-coupled device
MMA	-	Methyl methacrylate

Availability of data and materials
Not applicable

Ethics approval and consent to participate
Not applicable

Competing interests
The authors declare that they have no competing interests.

Consent for publication
Not applicable

Authors' contributions
The idea was conceived by Jackin, Sample systhesis and characterisation was conducted by Shirai and Kinashi, Optical experiments were done by Jackin, Shirai and Haginaka, Jackin wrote the manuscript, Sakai and Tsutsumi supervised the research.

Authors' information
Not applicable

Author details
[1]Materials Innovation Laboratory, Kyoto Institute of Technology, Kyoto, Japan. [2]Master's Programs of Materials Chemistry, Kyoto Institute of Technology, Kyoto, Japan. [3]Bachelor's Program of Materials Chemistry, Kyoto Institute of Technology, Kyoto, Japan. [4]Faculty of Materials Science and Engineering, Kyoto Institute of Technology, Kyoto, Japan.

References

1. Rosales-Guzmán, C., Bhebhe, N., Forbes, A.: Simultaneous generation of multiple vector beams on a single SLM. Optics Express **25**(21), 25697 (2017). doi:10.1364/OE.25.025697. Accessed 2021-11-17
2. Tang, Y., Perrie, W., Schille, J., Loeschner, U., Li, Q., Liu, D., Edwardson, S.P., Forbes, A., Dearden, G.: High-quality vector vortex arrays by holographic and geometric phase control. Journal of Physics D: Applied Physics **53**(46), 465101 (2020). doi:10.1088/1361-6463/ab9d9b. Accessed 2021-11-17
3. Zhang, N., Scaffardi, M., Klitis, C., Malik, M.N., Fresi, F., Zhu, J., Cai, X., Yu, S., Bogoni, A., Sorel, M.: Large-scale integrated reconfigurable orbital angular momentum mode multiplexer, 8
4. Du, J., Wang, J.: Design of On-Chip N-Fold Orbital Angular Momentum Multicasting Using V-Shaped Antenna Array. Scientific Reports **5**(1), 9662 (2015). doi:10.1038/srep09662. Accessed 2021-11-17
5. Cai, X., Wang, J., Strain, M.J., Johnson-Morris, B., Zhu, J., Sorel, M., O'Brien, J.L., Thompson, M.G., Yu, S.: Integrated Compact Optical Vortex Beam Emitters. Science **338**(6105), 363–366 (2012). doi:10.1126/science.1226528. Accessed 2021-11-17
6. Du, J., Wang, J.: Chip-scale optical vortex lattice generator on a silicon platform. Optics Letters **42**(23), 5054 (2017). doi:10.1364/OL.42.005054. Accessed 2021-11-17
7. Yue, F., Wen, D., Zhang, C., Gerardot, B.D., Wang, W., Zhang, S., Chen, X.: Multichannel Polarization-Controllable Superpositions of Orbital Angular Momentum States. Advanced Materials **29**(15), 1603838 (2017). doi:10.1002/adma.201603838. Accessed 2021-11-17

8. Maguid, E., Yulevich, I., Veksler, D., Kleiner, V., Brongersma, M.L., Hasman, E.: Photonic spin-controlled multifunctional shared-aperture antenna array, 6
9. Jin, J., Pu, M., Wang, Y., Li, X., Ma, X., Luo, J., Zhao, Z., Gao, P., Luo, X.: Multi-Channel Vortex Beam Generation by Simultaneous Amplitude and Phase Modulation with Two-Dimensional Metamaterial. Advanced Materials Technologies **2**(2), 1600201 (2017). doi:10.1002/admt.201600201. Accessed 2021-11-17
10. Ren, H., Briere, G., Fang, X., Ni, P., Sawant, R., Héron, S., Chenot, S., Vézian, S., Damilano, B., Brändli, V., Maier, S.A., Genevet, P.: Metasurface orbital angular momentum holography. Nature Communications **10**(1), 2986 (2019). doi:10.1038/s41467-019-11030-1. Accessed 2021-11-17
11. Jin, J., Li, X., Pu, M., Guo, Y., Gao, P., Xu, M., Zhang, Z., Luo, X.: Angular-multiplexed multichannel optical vortex arrays generators based on geometric metasurface. iScience **24**(2), 102107 (2021). doi:10.1016/j.isci.2021.102107. Accessed 2021-11-17
12. Huang, L., Song, X., Reineke, B., Li, T., Li, X., Liu, J., Zhang, S., Wang, Y., Zentgraf, T.: Volumetric Generation of Optical Vortices with Metasurfaces. ACS Photonics **4**(2), 338–346 (2017). doi:10.1021/acsphotonics.6b00808. Accessed 2021-11-17
13. Jin, J., Li, X., Pu, M., Ma, X., Luo, X.: Wavelength-Dependent Three-Dimensional Volumetric Optical Vortices Modulation Based on Metasurface. IEEE Photonics Journal **10**(6), 1–8 (2018). doi:10.1109/JPHOT.2018.2875779. Accessed 2021-11-23
14. Liu, J., Min, C., Lei, T., Du, L., Yuan, Y., Wei, S., Wang, Y., Yuan, X.-C.: Generation and detection of broadband multi-channel orbital angular momentum by micrometer-scale meta-reflectarray. Optics Express **24**(1), 212 (2016). doi:10.1364/OE.24.000212. Accessed 2021-11-17
15. Zhuang, Y., Yang, Q., Wu, P., Zhang, W., Ren, Y., Liu, H.: Vortex beam array generated by a volume compound fork grating in lithium niobite. Results in Physics **24**, 104083 (2021). doi:10.1016/j.rinp.2021.104083. Accessed 2021-11-17
16. Barboza, R., Bortolozzo, U., Clerc, M.G., Residori, S., Vidal-Henriquez, E.: Optical vortex induction via light–matter interaction in liquid-crystal media. Advances in Optics and Photonics **7**(3), 635 (2015). doi:10.1364/AOP.7.000635. Accessed 2021-11-23
17. Fuh, A.Y.G., Tsai, Y.-L., Yang, C.-H., Wu, S.T.: Fabrication of optical vortex lattices based on holographic polymer-dispersed liquid crystal films. Optics Letters **43**(1), 154 (2018). doi:10.1364/OL.43.000154. Accessed 2021-11-17
18. Carpentier, A.V., Michinel, H., Salgueiro, J.R., Olivieri, D.: Making optical vortices with computer-generated holograms. American Journal of Physics **76**(10), 916–921 (2008). doi:10.1119/1.2955792. Accessed 2021-11-17
19. Guo, Z., Qu, S., Liu, S.: Generating optical vortex with computer-generated hologram fabricated inside glass by femtosecond laser pulses. Optics Communications **273**(1), 286–289 (2007). doi:10.1016/j.optcom.2006.12.023. Accessed 2021-11-17
20. Kinashi, K., Nakanishi, I., Sakai, W., Tsutsumi, N.: Material Design of Azo-Carbazole Copolymers for Preservation Stability with Rewritable Holographic Stereograms. Macromolecular Chemistry and Physics **220**(2), 1800456 (2019). doi:10.1002/macp.201800456. Accessed 2021-12-02
21. Yoshikawa, H., Yamaguchi, T.: Review of Holographic Printers for Computer-Generated Holograms. IEEE Transactions on Industrial Informatics **12**(4), 1584–1589 (2016). doi:10.1109/TII.2015.2475722. Accessed 2021-11-26
22. Kinashi, K., Fukami, T., Yabuhara, Y., Motoishi, S., Sakai, W., Kawamoto, M., Sassa, T., Tsutsumi, N.: Molecular design of azo-carbazole monolithic dyes for updatable full-color holograms. NPG Asia Materials **8**(9), 311–311 (2016). doi:10.1038/am.2016.136. Accessed 2021-12-02